frontiers | Frontiers in Forests and Global Change

TYPE Original Research
PUBLISHED 28 March 2023
DOI 10.3389/ffgc.2023.1146742

OPEN ACCESS

EDITED BY
Philippe Tanguay,
Laurentian Forestry Centre, Natural Resources Canada, Canadian Forest Service, Canada

REVIEWED BY
Raiza Castillo,
University of Florida, United States
Carrie J. Fearer,
University of New Hampshire, United States

*CORRESPONDENCE
Cameron D. McIntire
✉ cameron.mcintire@usda.gov

SPECIALTY SECTION
This article was submitted to Pests, Pathogens and Invasions, a section of the journal Frontiers in Forests and Global Change

RECEIVED 17 January 2023
ACCEPTED 28 February 2023
PUBLISHED 28 March 2023

CITATION
McIntire CD (2023) Physiological impacts of beech leaf disease across a gradient of symptom severity among understory American beech.
Front. For. Glob. Change 6:1146742.
doi: 10.3389/ffgc.2023.1146742

Physiological impacts of beech leaf disease across a gradient of symptom severity among understory American beech

Cameron D. McIntire*

Forest Health Protection, USDA Forest Service, Durham, NH, United States

Beech leaf disease (BLD) damage is associated with the parasitic nematode *Litylenchus crenatae* ssp. *mccannii*. Foliar symptoms manifest as darkened or chlorotic galls in the interveinal portions in the leaf, which become leathery and crinkled under high severity of infection. Though nearly a decade has passed since the discovery of this disease, little is known regarding the impact of BLD on leaf function and physiology. This study assesses the variation in leaf gas exchange and physiological leaf traits among asymptomatic and BLD-infected leaves across a gradient of symptom severity within a natural forested stand in central Connecticut, USA. Leaves with BLD symptoms are found to have significantly reduced carbon assimilation and instantaneous water use efficiency, with increased levels of stomatal conductance as symptom severity progresses. Leaf response to light manipulation is also affected, with an increase in dark respiration and the light compensation point among banded and crinkled leaves. Additionally, BLD symptoms are found to have a significant influence on leaf water content, specific leaf area, and leaf nitrogen content. Relationships between gas exchange and these leaf traits yield linear correlations that are used to infer functional relationships impacted by the disease.

KEYWORDS

tree physiology, forest pathology, beech leaf disease, plant parasitic nematodes, leaf gas exchange, leaf traits, *Fagus grandifolia*, *Litylenchus crenatae mccannii*

Introduction

Beech leaf disease (BLD) is an emerging threat to native American beech (*Fagus grandifolia* L.) of North American forests. Since 2012, BLD has expanded from an initial discovery in Ohio to 12 states throughout the eastern United States and the Canadian province of Ontario. Disease progression has accelerated in recent years, with respect to both the widespread occurrence and the severity within chronically infected stands. A foliar parasitic nematode, *Litylenchus crenatae* subspecies *mccannii* (*Lcm*), is believed to be the primary causal agent of BLD. Readily observable symptoms of BLD infection vary based on the severity of foliar damage, which is thought to be a product of nematode populations at the time of leaf development within the bud. Generalized leaf deformities associated with other parasitic nematodes are known to induce the formation of neoplastic tissue and

galls, similar to those sometimes associated with mite damage (Palomares-Rius et al., 2017). The milder symptomology of BLD, commonly referred to as *banding*, consists of a gall formation within the interveinal portions of a leaf that appears as a discolored band, where the size and number of bands is somewhat random. The more severe symptom expression is referred to as *crinkling*, where a leaf appears shrunken and deformed, with a thickened leathery feel and often bearing chlorotic tissue. Unlike many fungal-borne foliar diseases, the symptoms of BLD do not progress throughout the duration of a growing season, such that the symptom presentation of individual leaves at the time of bud break is consistent through leaf senescence (Fearer et al., 2022b). Under a high severity of infection, thought to occur when nematode populations within the bud are exceptionally high, buds are aborted from the stem and leaves fail to flush out in the spring. In some instances, a secondary flush of leaves will occur later in the growing season. However, these second-flush leaves are often stunted and only account for a small fraction of foliage lost from the crown. At the tree level, BLD causes a marked increase in canopy transparency and branch dieback (Reed et al., 2022), which is hypothesized to have impacts on growth, vigor, and long-term survival.

Pests and diseases that result in a reduction of foliage are often associated with declines in woody diameter increment (Oliva et al., 2016; McIntire et al., 2018), and in the longer term, reductions in stored carbohydrates (Landhausser and Lieffers, 2012). Among residual symptomatic leaves, it is unknown how symptoms associated with BLD are altering leaf function. Given that BLD symptoms persist from year to year, measuring the direct impacts on leaf gas exchange is useful for understanding the compounding stress on carbon assimilation capacity. While nematode-induced tree diseases that affect roots [*Meloidogyne* spp., (Elling, 2013)] and stem wood [*Bursaphelenchus xylophilus*, (Kim et al., 2020)] have been well studied, little is known regarding how a novel foliar parasitic nematode impacts tree physiology. At the cellular level, *Lcm* can induce widespread damage to the mesophyll (Carta et al., 2020). This can lead to chlorosis-necrosis and is expected to negatively impact the photosynthetic function of these tissues. Furthermore, *Lcm* is known to cause deformation of stomata (Carta et al., 2020), the pores on the leaf surface responsible for regulating gas exchange. It is plausible that this mechanical damage alters carbon assimilation rates, stomatal conductance, and in turn, the water use efficiency of the leaf. The deterioration of mesophyll may also impact physical properties of the leaf that play a role in photosynthesis and the regulation of gas exchange. Identifying leaf traits that vary with BLD infection may serve as an indicator of relative disease severity, beyond a coarse grouping based on observations of leaf morphology.

The objectives of this study were to measure leaf gas exchange coupled with leaf trait data to quantify physiological impacts across a gradient of BLD severity. This was accomplished through a field experiment in three parts. First, leaf gas exchange was measured systematically across BLD symptom categories, assessing both responses to manipulated light intensity and *via* instantaneous measurements at a saturated light level. Second, leaves sampled in the field were collected for laboratory analysis of specific leaf area, leaf water content, and leaf nitrogen content. Finally, correlation between leaf traits and instantaneous gas exchanged was evaluated for functional relationships with respect to BLD severity.

Materials and methods

Study site and plant material

The experiment was conducted the Meshomasic State Forest, approximately 8 km west of Marlborough, Connecticut (41.6164 N, −72.5530 W, 164 m above sea level). The stand consists of mature American beech, white oak (*Quercus alba* L.), red oak (*Quercus rubra* L.), black birch (*Betula lenta* L.), and sugar maple (*Acer saccharum* Marshall). Stand basal area is 25 m^2 ha^{-1} with 502 trees per acre, estimated using a BAF 10 prism. American beech represents 26% of the total basal area and also dominates the understory of the stand. Symptoms of BLD were first observed in this stand in 2021 and are now present on all observed host trees. All trees exhibited a mild infestation of the scale insect *Cryptococcus fagisuga,* with a low occurrence of cankers associated with *Neonectria*, also known as beech bark disease (Houston, 1994). Cankers were observed primarily on mature trees in the overstory stratum but were not present on the understory trees sampled in this study.

Sampled trees (n = 12) in the understory stratum were selected at random inside a 0.4 ha area within the stand. All leaves were accessed from intact stem segments between 0.5 and 2.0 m above ground level. Tree diameter at breast height (DBH, 1.3 m above ground level) ranged from 2.2 to 21.1 cm with a mean of 9.1 cm (SD ± 5.4). Three BLD symptom categories were established based on the visual presentation of symptoms at the time of measurement: asymptomatic, banded, and crinkled (**Supplementary Figure 1**). Asymptomatic leaves are those which appear healthy with normal size, color, and without the presence of galls or necrotic tissue. Banded leaves are those with normal size but with the presence of galls that present as darkened bands that manifest in the interveinal portions of infected leaf surfaces. Crinkled leaves are diminutive with a darkened green color throughout and often exhibit areas if chlorotic and/or necrotic tissue. While BLD symptoms do occur on a natural continuous gradient, the banded and crinkled distinction is readily identifiable in the field and can be an indicator of disease severity that corresponds to nematode populations within the leaf (Fearer et al., 2022a).

Leaf gas exchange measurements

All field data was collected on 18 August 2022 between the hours of 830 and 1400 EST. Leaf gas exchange was measured on intact leaves while attached to the branch using an LI-6400 infrared gas analyzer equipped with a 6400-02B LED light source (LI-COR, Lincoln, NB, USA). Light response curves were derived from a subset of trees (n = 3) using a leaf from each symptom category per tree, where the photosynthetic photon flux density (PPFD) was manipulated at 10 setpoints: 2,000, 1,500, 1,000, 500, 250, 120, 60, 30, 15, and 0 μmmol m^{-2} s^{-1}. Instantaneous measurements of gas exchange were performed at a PPFD of 1000 μmmol m^{-2} s^{-1} and replicated on three leaves per symptom category on a subset of trees (n = 3) and averaged. To maximize the amount of tree replication in the campaign due to time limitation, instantaneous gas exchange was measured on a single leaf from each symptom category for all other trees (n = 9). Leaves were allowed to equilibrate in the

leaf chamber for 2–5 min before logging three measurements over a span of 10 s, the average of those instantaneous logs are reported throughout. The conditions within the leaf chamber were maintained at a CO_2 concentration of 415 μmmol mol^{-1}, a temperature of 22.1°C (SD ± 0.01), and relative humidity of 47.1% (SD ± 5.2). Individual leaf samples were harvested into plastic bags and transported on ice for laboratory analyses of leaf traits. A total of 81 leaves were collected (n = 27 per symptom type).

Leaf traits

Each sampled leaf was measured for specific leaf area (SLA, cm^2 g^{-1}), leaf water content (LWC,%), and nitrogen content (Leaf N,%). Fresh leaves were weighed on an electronic balance, then imaged on the adaxial surface using a flatbed scanner at 600 dpi resolution (Epson Expression 12000XL, Nagano, Japan). Leaves were then oven dried at 60°C for 72 h and measured for dry mass. Total leaf area was determined using a protocol developed for the ImageJ software. The SLA is calculated as the ratio of total leaf area to dry mass. The LWC is calculated as:

$$LWC = \left(\frac{fresh\ mass\ -\ dry\ mass}{fresh\ mass}\right)\ 100$$

For leaf N analysis, whole dried leaves were ground to a homogonous powder using a mini Wiley Mill and passed through a 0.85 mm sieve (#20 mesh), followed by mortar and pestle. Ground samples were dried for an additional 24 h at 60°C. Aliquots of 2.0–5.0 mg dry mass were sealed in tin capsules and measured using a Flash EA 1112 elemental analyzer (Thermo Fisher Scientific, Waltham, MA, USA).

Statistical analyses

All statistical analysis and data visualizations were performed in R studio (version 4.0.2, R Foundation for Statistical Computing, Vienna, Austria). Light response curves were fit with a non-rectangular hyperbola model (Marshall and Biscoe, 1980) using the package "photosynthesis" (Stinziano et al., 2020). From these curve fits, estimates of light-saturated CO_2 assimilation (A_{max}), dark respiration rate (R_d), light compensation point (Γi), and apparent quantum yield (α) were derived. For instantons gas exchange measurements, the net assimilation rate (A_{net}), stomatal conductance (g_s), and intrinsic water use efficiency (A_{net}/g_s or δ) were evaluated. A one-way analysis of variance (ANOVA) was used determine significant effects ($p \leq 0.05$) attributed to observed BLD symptoms for each variable. *Post-hoc* contrasts between symptom categories were analyzed *via* a Tukey test using the estimated marginal means with the package "emmeans" (Lenth et al., 2018). Similarly, foliar trait data for LWC, SLA, and leaf N were analyzed by symptom category with one-way ANOVA and a Tukey's *post-hoc* test, using the mean of all leaves measured for each tree (n = 12).

Linear regression models were developed to evaluate relationships between A_{net}, g_s, and δ with foliar functional traits as dependent variables (LWC, SLA, and leaf N) by symptom category. Analysis of covariance (ANCOVA) was used to determine significant differences for interactions between leaf traits and symptom categories. To assess the interaction between the covariate and factor variables, significant differences in slopes of the covariate trend for each symptom category were evaluated with the "emtrends" function.

Results

Light response curves

Photosynthetic response to light varied by BLD symptom category (Table 1 and Figure 1). Compared to asymptomatic leaves, values of A_{max} were 25.9 and 23.6% lower in banded and crinkled leaves, respectively. However, these differences were not found to be significant (Table 1), in part due to a high amount of variability in carbon assimilation rates among asymptomatic leaves at high levels of light (PPFD > 1000 μmol m^{-2} s^{-1}). Leaf symptoms had a significant effect on both R_d [$F(2,6) = 9.21$, $p = 0.015$] and Γ_i [$F(2,6) = 7.58$, $p = 0.023$]. Estimates of R_d for asymptomatic leaves was nearly zero, while banded and crinkled leaves respired at a rate of 0.46 and 0.80 μmol m^{-2} s^{-1}, respectively. Similarly, Γ_i was higher among diseased leaves, where the compensation point was estimated at 0.23, 5.50, and 20.69 μmol m^{-2} s^{-1} among asymptomatic, banded, and crinkled leaves, respectively. No differences in α were found between leaf symptom categories.

Instantaneous gas exchange

Leaf symptoms influenced all metrics of gas exchanged evaluated in this study (Table 1 and Figure 2). Estimates of A_{net} were significantly lower in both banded and crinkled leaves with respect to asymptomatic leaves [$F(2,33) = 40.16$, $p < 0.001$]. *Post-hoc* analysis found both disease symptoms to be significantly lower than asymptomatic leaves ($p < 0.001$), but no difference between the banded and crinkled symptoms ($p = 0.115$; Figure 2A). Compared to asymptomatic leaves, A_{net} of banded and crinkled leaves was 40.7 and 53.3% lower, respectively. The highest A_{net} measured among individual leaves was 4.7 μmol CO_2 m^{-2} s^{-1} (Tree 7, asymptomatic) and the lowest was 0.8 μmol CO_2 m^{-2} s^{-1} (Tree 6, crinkled). Estimates of g_s are significantly different by symptom category [$F(2,33) = 11.68$, $p < 0.001$]. *Post-hoc* analysis found that conductance of crinkled leaves was significantly higher than either symptom category ($p \leq 0.001$, Figure 2B), an increase of 60% with respect to asymptomatic leaves. Estimates of δ were significantly different by symptom category [$F(2,33) = 75.59$, $p < 0.001$]. *Post-hoc* analysis found that δ differed significantly between each leaf symptom ($p < 0.001$, Figure 2C), such that compared to asymptomatic leaves, δ was 34.7 and 67.6% lower among banded and crinkled leaves, respectively.

Leaf traits

Progression of leaf symptoms evoked differences in LWC, SLA, and leaf N (Table 1 and Figure 3). Measured LWC was significantly

TABLE 1 Means ± standard deviation for leaf traits of light-saturated photosynthetic rate (A_{max}; μmol m^{-2} s^{-1}), dark respiration rate (R_d; μmol m^{-2} s^{-1}), light compensation point (Γ_i; μmol m^{-2} s^{-1}), apparent quantum yield (α), instantaneous net carbon assibilation rate (A_{net}; μmol m^{-2} s^{-1}), stomatal conductance (g_s; mol m^{-2} s^{-1}), intrinsic water use efficiency (δ; μmol CO_2 mol^{-1} H_2O), leaf water content (LWC,%), specific leaf area (SLA, cm^2 g^{-1}), and leaf nitrogen content (Leaf N,%).

	Symptom category			ANOVA			
	Asymptomatic	Banded	Crinkled	*n*	df	*F*-value	*p*-Value
A_{max}	3.13 ± 0.49^a	2.32 ± 0.06^a	2.39 ± 0.45^a	3	2	3.99	0.079
R_d	0.01 ± 0.02^a	0.46 ± 0.28^{ab}	0.80 ± 0.27^b	3	2	9.21	0.015
Γ_i	0.23 ± 0.40^a	5.50 ± 2.58^a	20.69 ± 11.28^a	3	2	7.58	0.023
α	0.06 ± 0.02^a	0.10 ± 0.05^{ab}	0.07 ± 0.03^b	3	2	1.20	0.364
A_{net}	3.66 ± 0.64^a	2.17 ± 0.42^b	1.71 ± 0.59^b	12	2	40.16	<0.001
g_s	0.05 ± 0.01^a	0.05 ± 0.01^a	0.08 ± 0.03^b	12	2	11.68	<0.001
δ	74.74 ± 9.95^a	48.77 ± 9.88^b	24.21 ± 10.37^c	12	2	75.59	<0.001
LWC	58.91 ± 1.07^a	63.00 ± 1.63^b	66.76 ± 3.12^c	12	2	41.12	<0.001
SLA	394.77 ± 28.99^a	266.86 ± 37.33^b	152.96 ± 21.42^c	12	2	195.60	<0.001
Leaf N	1.90 ± 0.18^a	2.01 ± 0.23^{ab}	2.16 ± 0.22^b	12	2	5.39	0.009

ANOVA indicates number of replicates used in analysis (*n*), degrees of freedom (df), *F*-value and *p*-value results for comparisons between symptom categories. Statistical differences determined *via* Tukey *post-hoc* analysis are indicated by difference in letters (^{a}, ^{b}, ^{c}) between symptom groups for each response variable.

different by symptom category [$F(2,33) = 41.12$, $p < 0.001$]. *Post-hoc* analysis found significant differences of LWC between each leaf symptom ($p < 0.001$, Figure 3A), where with respect to asymptomatic leaves, water content increased by 6.9% among banded leaves and 13.3% among crinkled leaves. Measured SLA was also significantly different by symptom category [$F(2,33) = 195.60$, $p < 0.001$]. *Post-hoc* analysis found significant differences of SLA between each leaf symptom ($p < 0.001$, Figure 3B), where with respect to asymptomatic leaves, SLA was reduced by 32.4% among banded leaves and 61.2% among crinkled leaves. Total leaf N was also impacted by leaf symptomology [$F(2,33) = 5.39$, $p = 0.009$], where crinkled leaves exhibit significantly higher N on a dry mass basis compared to asymptomatic leaves ($p = 0.007$, Figure 3C). The total leaf N among asymptomatic leaves was 1.90%, with crinkled leaves at 2.16%, a relative increase of 13.7%. Measured N values of banded leaves were intermediate between the other symptom categories and not significantly different from either asymptomatic or crinkled leaves.

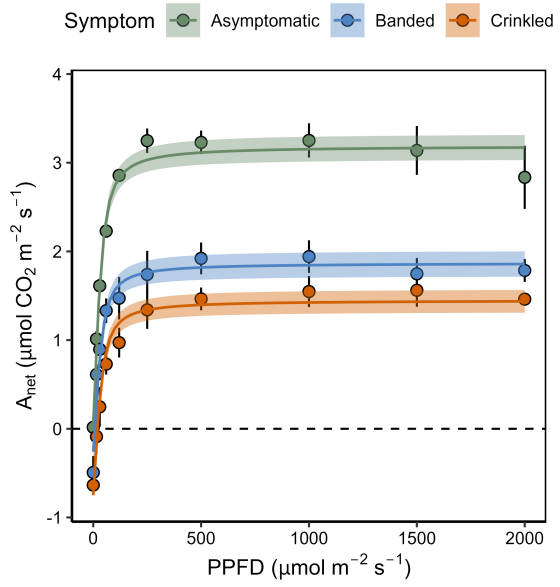

FIGURE 1
Net carbon assibilation rate (A_{net}) as a function of the photosynthetic photon flux density (PPFD) by BLD symptom category. Points show mean and standard error ($n = 3$), shaded region is the 95% confidence interval for the non-rectangular hyperbola model.

Functional relationships between leaf traits and gas exchange

Linear regression analysis revealed correlations between leaf trait data and instantaneous gas exchange. Photosynthesis had an overall negative linear relationship to LWC (Figure 4A) and Leaf N (Figure 4C), but a positive relationship to SLA (Figure 4B) across all symptom categories. Within symptom categories A_{net} was found to decline as function of SLA, in contrast to the across-group relationship, though ANCOVA found no significant difference in slopes between symptoms [$F(2,30) = 1.19$, $p = 0.319$]. Response of g_s as a function of LWC (Figure 4D) and leaf N (Figure 4F) did not yield significant correlations ($p > 0.05$). A significant negative correlation between g_s and SLA was found (Figure 4E), with a significant difference in slopes between leaf symptom categories [$F(2,30) = 5.297$, $p = 0.011$]. *Post-hoc* comparisons indicated that g_s of crinkled leaves decline more rapidly with increasing SLA (slope = -9.36×10^{-4}) with respect to both banded leaves (slope = 1.18×10^{-4}, $p = 0.009$) and asymptomatic leaves (slope = 1.82×10^{-4}, $p = 0.028$). This was the only trait relationship for which ANVOA revealed a significant difference between symptom categories. Measurements of δ exhibited a strong negative correlation with LWC (Figure 4G), a strong negative correlation with SLA (Figure 4H), and a weak but significant negative correlation with leaf N (Figure 4I). Coefficient of determination

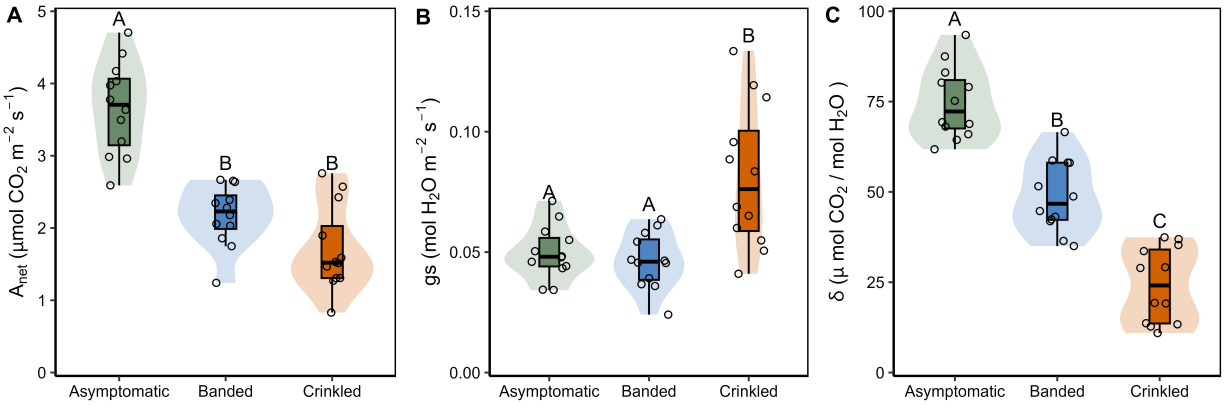

FIGURE 2
(A) Instantaneous net carbon assibilation rate (A_{net}); **(B)** stomatal conductance (g_s); and **(C)** intrinsic water use efficiency (δ) by BLD symptom category. Box plots show Q25–1.5 IQR, Q25, Q50, Q75, and Q75 + 1.5 IQR values, the shaded region is the continuous density distribution, and open circles are tree replicates (n = 12). Statistical differences are indicated by different letters between symptom categories (Tukey *post-hoc* analysis, $p < 0.05$).

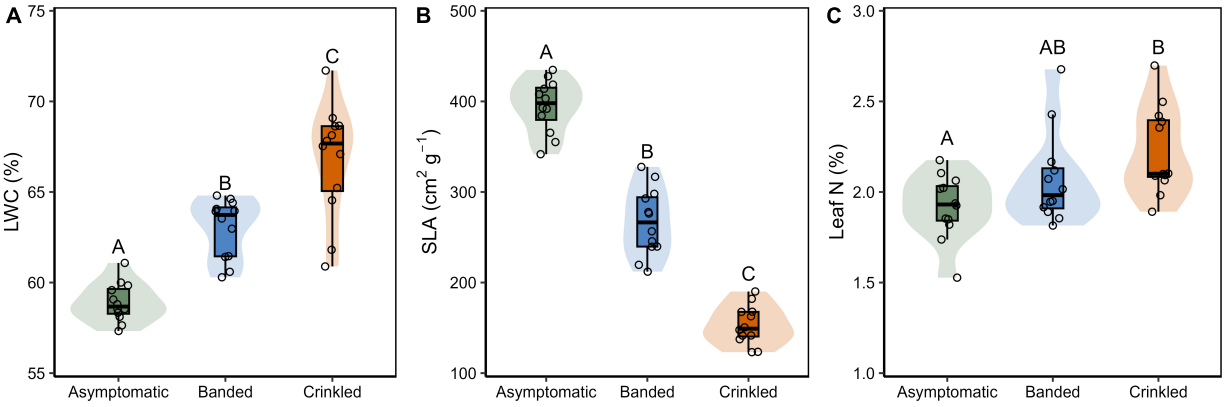

FIGURE 3
(A) Leaf water content (LWC); **(B)** specific leaf area (SLA); and **(C)** leaf N content by BLD symptom category. Box plots show Q25–1.5 IQR, Q25, Q50, Q75, and Q75 + 1.5 IQR values, the shaded region is the continuous density distribution, and open circles are tree replicates (n = 12). Statistical differences are indicated by different letters between symptom categories (Tukey *post-hoc* analysis, $p < 0.05$).

(R^2) and p-values across symptom linear regressions are shown within the panels of Figure 4.

Discussion

Light curve outputs that are significantly altered due to BLD symptoms are R_d and Γi, both of which are relevant under low and no-light conditions. The increased rates of R_d among diseased leaves suggests that stomates may not be able to close effectively, which is supported in part by the increased rates of g_s measured in leaves with the crinkled symptomology. Concerning Γ_i, the point where the rate of photosynthesis is equal to the rate of respiration, symptomatic leaves require a higher PPFD. A functional explanation for this finding may be attributed to changes in the cellular structure within infected leaves, specifically, a thickening and tighter arrangement of the palisade and spongey mesophyll cells. Under natural conditions, a thickening of the mesophyll can be correlated with Γ_i as leaf age progresses among non-deciduous hardwood species (Ashton and Turner, 1979). Canopy light exposure is also known to influence this compensation point, where a vertical gradient of diminishing photosynthetically active radiation causes trees to produce shade leaves in the lower crown that tend to be thinner (i.e., fewer mesophyll layers) with a lower Γi, whereas leaves near the top of the canopy are comparatively thicker with a higher Γi due to a greater intensity and availability of PPFD (Lewis et al., 2000; Norby et al., 2003). Leaves infected with BLD, especially those with crinkled symptomology, appear to be more anatomically similar to leaves that would be exposed to full sun, and thus require higher light intensity before carbon assimilation surpasses respiration. However, this comparison to sun exposed foliage does not hold true with regards to photosynthetic productivity, where such leaves would typically yield higher values of A_{net}. Instead, symptomatic leaves exhibit significantly lower rates of carbon assimilation compared to neighboring asymptomatic leaves. This loss of function is reflected in the instantaneous gas exchange measured under

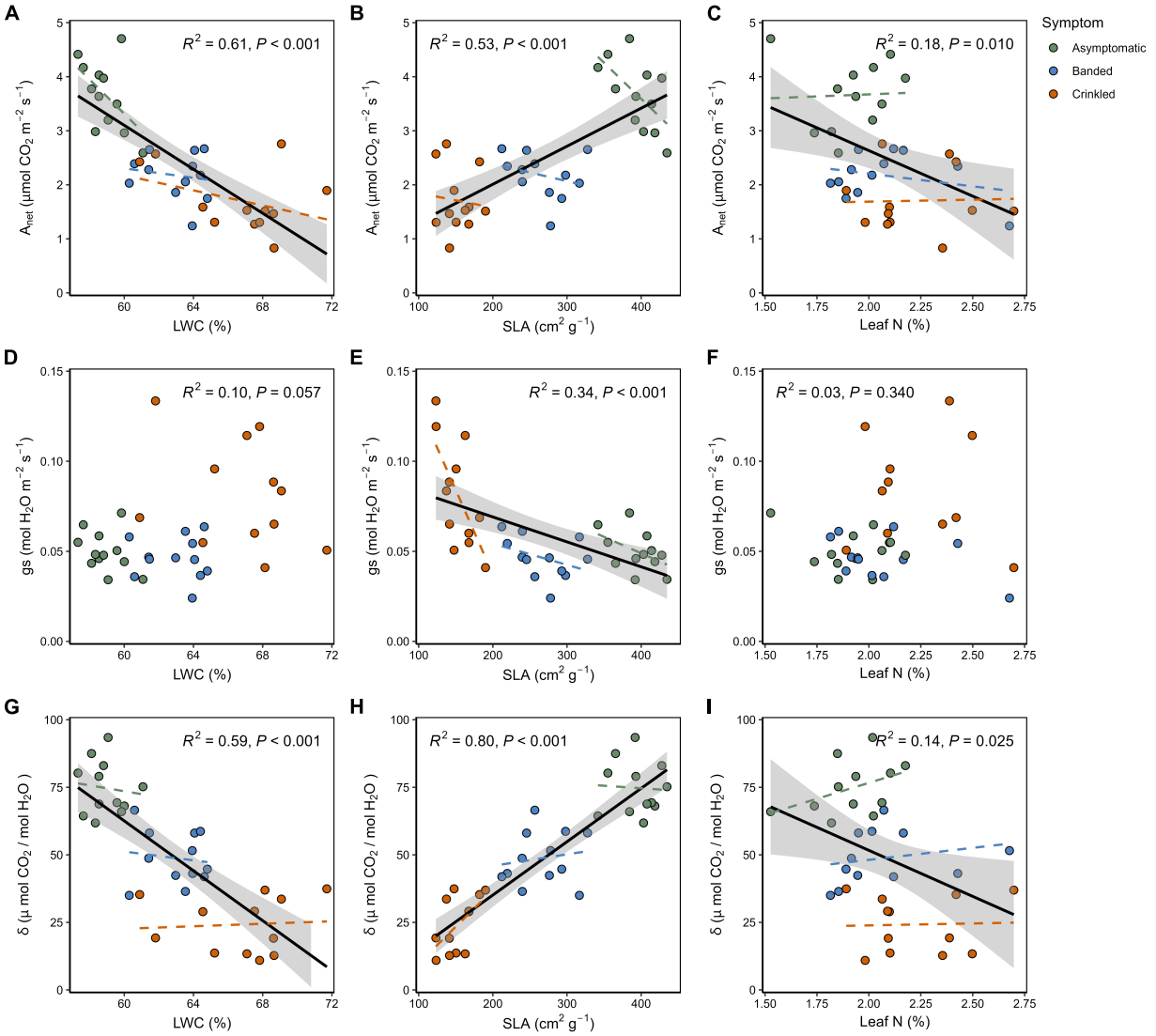

FIGURE 4
Continuous relationships between leaf treats and measured gas exchange: **(A)** A_{net} as a function of LWC; **(B)** A_{net} as a function of SLA, **(C)** A_{net} as a function of leaf N; **(D)** g_s as a function of LWC; **(E)** g_s as a function of SLA; **(F)** g_s as a function of leaf N; **(G)** δ as a function of LWC; **(H)** δ as a function of SLA; **(I)** δ as a function of leaf N. Black lines show the overall linear regressions across all symptom categories with the shaded region indicating the 95% confidence interval. Dashed colored lines show linear regressions within the respective symptom categories. Overall regression lines are omitted where not found significant ($p > 0.05$).

constant light conditions (1,000 µmmol m^{-2} s^{-1}) of this study.

Overall values of A_{net} are quite low, peaking at 4.7 µmol CO_2 m^{-2} s^{-1} for an asymptomatic leaf. This was anticipated given the understory canopy position of sampled trees, as well as the known shade tolerance of this species (Nyland et al., 2006). A comparable field study reports A_{max} of 2.9–3.1 µmol CO_2 m^{-2} s^{-1} among understory beech seedlings and roots sprouts, respectively (Farahat and Lechowicz, 2013), while A_{net} of light saturated codominant beech has been measured to range from 7.1 to 8.7 µmol CO_2 m^{-2} s^{-1} (Elvir et al., 2006). As a consequence of the shade regime, light manipulation of gas exchange revealed that A_{net} begins to taper at relatively low light levels (PPFD ≈ 500 µmol m^{-2} s^{-1}). A_{net} declines as a function of leaf N across all symptoms of BLD, contrary to the positive relationship that is generally found across tree species and functional types (Evans, 1989; Kattge et al., 2009). This finding is interesting given that crinkled leaves exhibit significantly higher leaf N (2.16%) compared to asymptotic leaves (1.90%), suggesting that mechanical damage to the photosystem outweighs any functional benefit of increased N content. Other studies have reported values for American beech leaf N on the order of 1.76% among root spouts (Farahat and Lechowicz, 2013), and from 2.14 to 2.47% among codominant trees (Elvir et al., 2006). Although leaf N can be influenced by site factors such as climate, elevation, and soil type (Gong et al., 2020), the variation measured in this study can clearly be attributed to disease symptoms given the close proximity of sampled trees.

Higher and more variable values of g_s measured among crinkled leaves resulted in a significantly diminished δ, where δ

among asymptomatic leaves is three-fold higher in comparison. This shift in water use efficiency at the leaf level has the potential to become problematic for maintaining stem xylem conductivity, in part due to the loss of foliage caused by BLD. Defoliation increases the leaf area to sapwood area ratio of trees (Kono et al., 2019), which can apply greater strain for maintaining hydraulic conductance (Mencuccini et al., 2019a,b). Controlled defoliation of balsam poplar (*Populus balsamifera* L.) is shown to reduce xylem-specific conductivity while increasing the vulnerability to cavitation among defoliated trees (Hillabrand et al., 2019). Furthermore, the risk of hydraulic failure is amplified as soil water becomes limiting (Brodribb and Cochard, 2009; Plaut et al., 2012; Sevanto et al., 2014), such is the case during seasonal droughts which are forecasted to become a more common phenomenon throughout the northeastern US (Hayhoe et al., 2007; Xue and Ullrich, 2022). Indeed, at the time of this study, 86% of the land area within the state of Connecticut was amid a severe drought, with an additional 13% classified as experiencing extreme drought (US Drought Monitor, 2022), inducing a wilting response among more sensitive tree species and those inhabiting shallow soils. As residual leaves infected with BLD exhibit greater water loss per unit carbon gained, the compounding stress of such drought events are likely to accelerate branch dieback and mortality. Further research to investigate the hydraulic traits of leaves symptomatic for BLD, and their associated branch segments, will be useful to elucidate the drought sensitivity among infected beech trees.

This work also demonstrates that SLA varies significantly within the BLD symptom categories, and therefore may serve as a proxy for quantifying disease severity on a continuous scale. The degree of separation in the SLA data is such that there is no overlap between the three symptom categories, while the variation within categories can likely be attributed to the degree of internal damage induced by parasitic nematode feeding. A study which evaluated the spectral properties of American beech leaves identified near-infrared bands that can be used to discriminate BLD symptom types and that symptom severity was associated with *Lcm* populations verified through both molecular techniques (qPCR) and counting *ex situ* nematodes (Fearer et al., 2022a). Measurements of SLA coupled with a direct estimate of *Lcm* populations within a leaf could be investigated to further explore this relationship.

The measured increase in LWC can be associated with cellular proliferation caused by damage induced while leaves are developing in the bud, leading to upregulated mesophyll cell production and presumably a higher abundance of vacuoles. Supporting evidence for this can be found among other plant parasitic nematodes in the Anguinidae family that are known stimulate cellular division and vacuolization (Stynes and Bird, 1982; Vovlas et al., 2016). Elevated LWC may also facilitate a more favorable environment for *Lcm*, as nematodes are generally reliant on hydric conditions throughout their lifecycle (Perry, 1999). Similarly, an increased leaf thickness caused by *Lcm* damage can also account for the reduced SLA as BLD symptom severity progresses. In other words, a thicker mesophyll coupled with a smaller total area, results in a denser and more hydrated leaf. It is notable that a higher water content was measured in crinkled leaves despite the presence of some necrotic and chlorotic tissue, which are generally presumed to be much drier areas of the leaf. The SLA is also linked to leaf function, as a positive linear relationship between SLA and A_{net} is well established for many hardwood tree species (Reich et al., 1998). This correlation is found to be significant across trees sampled in this study (**Figure 4B**), however, negative correlations were found within each BLD symptom category. The SLA is also found to be a strong predictor variable for g_s and δ across BLD symptom categories, emphasizing the role of this leaf trait in regulating gas exchange between leaf and atmosphere. The relationship of SLA to g_s shows that, within symptom categories, crinkled leaves exhibit a steeper negative slope that is significantly different from both banded and asymptomatic leaves. This may be partially explained by the stomatal deformations that have been reported in association with these advanced symptoms (Carta et al., 2023), resulting in poor stomatal closure and higher levels of g_s over the leaf surface. Naturally, differences in stomatal size and shape dictates mechanical function (Franks and Farquhar, 2007), while deformed stomates can alter the function of guard cells with respect to a healthy leaf (Ziv and Ariel, 1994).

This study did not assess the physiology of second-flush leaves that are associated within severely BLD-infected stands. Among trees that exhibit bud abortion, this second cohort of asymptomatic leaves was observed throughout the eastern US during the 2022 growing season. While these leaves may not harbor nematodes, they are markedly different from healthy leaves, appearing smaller and lighter in color. As a result, trees with a large quantity of aborted buds mimic trees that have undergone a defoliation event, though it should be noted that these thinned canopies were not foliated at the outset of the growing season and are colloquially referred to as "non-foliated." Furthermore, it would be meaningful to measure leaf traits in American beech trees that exhibit no symptoms of BLD to determine if there is a difference between asymptomatic leaves within an infected tree comparable within a tree that is void of disease. Many tree species demonstrate a compensatory response to defoliation *via* an upregulation of photosynthesis (Reich et al., 1993; Williams et al., 2016; McIntire et al., 2020), thus it's feasible that residual leaves within diseased American beech trees attempt to account for a net loss of carbohydrate. The compounding stress induced by multiple years of carbon limitation associated with BLD may become a consequential factor for inciting tree mortality, especially when coupled with other pests, diseases, and environmental elements.

Conclusion

Given the abundance and ecological value of American beech on the North American landscape, the impacts of BLD on tree health is a major concern for landowners and forest practitioners. The symptoms associated with BLD are shown to influence leaf gas exchange and physiological leaf traits that are linked to carbon assimilation capacity. Implications of these results point toward a compromised tree carbon budget, which can negatively affect growth, vigor, and long-term survival. Future work to build upon these findings should focus on assessing disease response among mature trees, second-flush leaves, and exploring the hydraulic sensitivity of BLD-infected American beech.

Data availability statement

Data pertaining to this study is available at Zenodo: https://zenodo.org/record/7612843#.Y-EzRnbMJZc.

Author contributions

The author confirms sole responsibility for the study conception and design, data collection, analysis and interpretation of results, and manuscript preparation.

Funding

This study was supported by the United States Department of Agriculture Forest Service, Region 9, State, Private and Tribal, Forestry, Forest Health and Forest Markets.

Acknowledgments

I thank Dr. Robert Marra for his assistance with selecting a suitable location to conduct this study and his continued efforts with the BLD long-term monitoring network. I also thank Emma Irvine and Jeff Merriam assisted with processing leaf samples for elemental analysis.

Conflict of interest

The author declares that the research was conducted in the absence of any commercial or financial relationships that could be construed as a potential conflict of interest.

Publisher's note

Supplementary material

The Supplementary Material for this article can be found online at: https://www.frontiersin.org/articles/10.3389/ffgc.2023.1146742/full#supplementary-material

References

Ashton, D., and Turner, J. (1979). Studies on the light compensation point of *Eucalyptus regnans* F. Muell. *Aust. J. Bot.* 27, 589–607. doi: 10.1071/BT9790589

Brodribb, T. J., and Cochard, H. (2009). Hydraulic failure defines the recovery and point of death in water-stressed conifers. *Plant Physiol.* 149, 575–584. doi: 10.1104/pp.108.129783

Carta, L. K., Handoo, Z. A., Li, S., Kantor, M., Bauchan, G., Mccann, D., et al. (2020). Beech leaf disease symptoms caused by newly recognized nematode subspecies *Litylenchus crenatae mccannii* (*Anguinata*) described from *Fagus grandifolia* in North America. *For. Pathol.* 50, 1–15. doi: 10.1111/efp.12580

Carta, L. K., Li, S., and Mowery, J. (2023). Beech leaf disease (BLD), *Litylenchus crenatae* and its potential microbial virulence factors. *For. Microbiol.* 3, 183–192. doi: 10.1016/B978-0-443-18694-3.00018-3

Elling, A. A. (2013). Major emerging problems with minor *Meloidogyne* species. *Phytopathology* 103, 1092–1102. doi: 10.1094/PHYTO-01-13-0019-RVW

Elvir, J. A., Wiersma, G. B., Day, M. E., Greenwood, M. S., and Fernandez, I. J. (2006). Effects of enhanced nitrogen deposition on foliar chemistry and physiological processes of forest trees at the Bear Brook Watershed in Maine. *For. Ecol. Manag.* 221, 207–214. doi: 10.1016/j.foreco.2005.09.022

Evans, J. R. (1989). Photosynthesis and nitrogen relationships in leaves of C_3 plants. *Oecologia* 78, 9–19. doi: 10.1007/BF00377192

Farahat, E., and Lechowicz, M. J. (2013). Functional ecology of growth in seedlings versus root sprouts of *Fagus grandifolia* Ehrh. *Trees* 27, 337–340. doi: 10.1007/s00468-012-0781-9

Fearer, C. J., Volk, D., Hausman, C. E., and Bonello, P. (2022b). Monitoring foliar symptom expression in beech leaf disease through time. *For. Pathol.* 52:e12725. doi: 10.1111/efp.12725

Fearer, C. J., Conrad, A. O., Marra, R. E., Georskey, C., Villari, C., Slot, J., et al. (2022a). A combined approach for early in-field detection of beech leaf disease using near-infrared spectroscopy and machine learning. *Front. For. Glob. Chang.* 5:934545. doi: 10.3389/ffgc.2022.934545

Franks, P. J., and Farquhar, G. D. (2007). The mechanical diversity of stomata and its significance in gas-exchange control. *Plant Physiol.* 143, 78–87. doi: 10.1104/pp.106.089367

Gong, H., Li, Y., Yu, T., Zhang, S., Gao, J., Zhang, S., et al. (2020). Soil and climate effects on leaf nitrogen and phosphorus stoichiometry along elevational gradients. *Glob. Ecol. Conserv.* 23:e01138. doi: 10.1016/j.gecco.2020.e01138

Hayhoe, K., Wake, C. P., Huntington, T. G., Luo, L., Schwartz, M. D., Sheffield, J., et al. (2007). Past and future changes in climate and hydrological indicators in the US Northeast. *Clim. Dyn.* 28, 381–407. doi: 10.1007/s00382-006-0187-8

Hillabrand, R. M., Hacke, U. G., and Lieffers, V. J. (2019). Defoliation constrains xylem and phloem functionality. *Tree Physiol.* 39, 1099–1108. doi: 10.1093/treephys/tpz029

Houston, D. R. (1994). Major new tree disease epidemics: Beech bark disease. *Annu. Rev. Phytopathol.* 32, 75–87. doi: 10.1146/annurev.py.32.090194.000451

Kattge, J., Knorr, W., Raddatz, T., and Wirth, C. (2009). Quantifying photosynthetic capacity and its relationship to leaf nitrogen content for global-scale terrestrial biosphere models. *Glob. Change Biol.* 15, 976–991. doi: 10.1111/j.1365-2486.2008.01744.x

Kim, B.-N., Kim, J. H., Ahn, J.-Y., Kim, S., Cho, B.-K., Kim, Y.-H., et al. (2020). A short review of the pinewood nematode, *Bursaphelenchus xylophilus*. *Toxicol. Environ. Health Sci.* 12, 297–304. doi: 10.1007/s13530-020-00068-0

Kono, Y., Ishida, A., Saiki, S. T., Yoshimura, K., Dannoura, M., Yazaki, K., et al. (2019). Initial hydraulic failure followed by late-stage carbon starvation leads to drought-induced death in the tree Trema orientalis. *Commun. Biol.* 2, 1–9. doi: 10.1038/s42003-018-0256-7

Landhausser, S. M., and Lieffers, V. J. (2012). Defoliation increases risk of carbon starvation in root systems of mature aspen. *Trees* 26, 653–661. doi: 10.1007/s00468-011-0633-z

Lenth, R., Singmann, H., Love, J., Buerkner, P., and Herve, M. (2018). *Emmeans: Estimated marginal means, aka least-squares means. R package version, 1. 3.*

Lewis, J., Mckane, R., Tingey, D., and Beedlow, P. (2000). Vertical gradients in photosynthetic light response within an old-growth Douglas-fir and western hemlock canopy. *Tree Physiol.* 20, 447–456. doi: 10.1093/treephys/20.7.447

Marshall, B., and Biscoe, P. (1980). A model for C3 leaves describing the dependence of net photosynthesis on irradiance. *J. Exp. Bot.* 31, 29–39. doi: 10.1093/jxb/31.1.29

McIntire, C. D., Huggett, B. A., Dunn, E., Munck, I. A., Vadeboncoeur, M. A., and Asbjornsen, H. (2020). Pathogen-induced defoliation impacts on transpiration, leaf gas exchange, and non-structural carbohydrate allocation in eastern white pine (*Pinus strobus*). *Trees* 35, 357–373. doi: 10.1007/s00468-020-02037-z

McIntire, C. D., Munck, I. A., Vadeboncoeur, M. A., Livingston, W. H., and Asbjornsen, H. (2018). Impacts of white pine needle damage on seasonal litterfall dynamics and wood growth of eastern white pine (*Pinus strobus*) in northern New England. *For. Ecol. Manag.* 423, 27–36. doi: 10.1016/j.foreco.2018.02.034

Mencuccini, M., Rosas, T., Rowland, L., Choat, B., Cornelissen, H., Jansen, S., et al. (2019b). Leaf economics and plant hydraulics drive leaf : Wood area ratios. *New Phytol.* 224, 1544–1556. doi: 10.1111/nph.15998

Mencuccini, M., Manzoni, S., and Christoffersen, B. (2019a). Modelling water fluxes in plants: From tissues to biosphere. *New Phytol.* 222, 1207–1222.

Norby, R. J., Sholtis, J. D., Gunderson, C. A., and Jawdy, S. S. (2003). Leaf dynamics of a deciduous forest canopy: No response to elevated CO2. *Oecologia* 136, 574–584. doi: 10.1007/s00442-003-1296-2

Nyland, R. D., Bashant, A. L., Bohn, K. K., and Verostek, J. M. (2006). Interference to hardwood regeneration in northeastern North America: Ecological characteristics of American beech, striped maple, and hobblebush. *North. J. Appl. For.* 23, 53–61. doi: 10.1093/njaf/23.1.53

Oliva, J., Stenlid, J., Grönkvist-Wichmann, L., Wahlström, K., Jonsson, M., Drobyshev, I., et al. (2016). Pathogen-induced defoliation of Pinus sylvestris leads to tree decline and death from secondary biotic factors. *For. Ecol. Manag.* 379, 273–280. doi: 10.1016/j.foreco.2016.08.011

Palomares-Rius, J. E., Escobar, C., Cabrera, J., Vovlas, A., and Castillo, P. (2017). Anatomical alterations in plant tissues induced by plant-parasitic nematodes. *Front. Plant Sci.* 8:1987. doi: 10.3389/fpls.2017.01987

Perry, R. (1999). Desiccation survival of parasitic nematodes. *Parasitology* 119, S19–S30. doi: 10.1017/S0031182000084626

Plaut, J. A., Yepez, E. A., Hill, J., Pangle, R., Sperry, J. S., Pockman, W. T., et al. (2012). Hydraulic limits preceding mortality in a piñon–juniper woodland under experimental drought. *Plant Cell Environ.* 35, 1601–1617. doi: 10.1111/j.1365-3040.2012.02512.x

Reed, S. E., Volk, D., Martin, D. K. H., Hausman, C. E., Macy, T., Tomon, T., et al. (2022). The distribution of beech leaf disease and the causal agents of beech bark disease (*Cryptoccocus fagisuga*, *Neonectria faginata*, N. ditissima) in forests surrounding Lake Erie and future implications. *For. Ecol. Manag.* 503:119753.

Reich, P. B., Walters, M. B., Krause, S. C., Vanderklein, D. W., Raffs, K. F., and Tabone, T. (1993). Growth, nutrition and gas exchange of *Pinus resinosa* following artificial defoliation. *Trees* 7, 67–77. doi: 10.1007/BF00225472

Reich, P., Ellsworth, D., and Walters, M. (1998). Leaf structure (specific leaf area) modulates photosynthesis–nitrogen relations: Evidence from within and across species and functional groups. *Funct. Ecol.* 12, 948–958.

Sevanto, S., Mcdowell, N. G., Dickman, L. T., Pangle, R., and Pockman, W. T. (2014). How do trees die? A test of the hydraulic failure and carbon starvation hypotheses. *Plant Cell Environ.* 37, 153–161. doi: 10.1111/pce.12141

Stinziano, J., Roback, C., Gamble, D., Murphy, B., Hudson, P., and Muir, C. (2020). *Photosynthesis: tools for plant ecophysiology & modeling. R package version, 2.*

Stynes, B. A., and Bird, A. F. (1982). Development of galls induced in *Lolium rigidum* by *Anguina agrostis*. *Phytopathology* 72, 336–346.

US Drought Monitor (2022). *Connecticut Drought Monitor Map Archive*. Available online at: https://droughtmonitor.unl.edu/ (accessed December 12, 2022).

Vovlas, N., Troccoli, A., Palomares-Rius, J. E., De Luca, F., Cantalapiedra-Navarrete, C., Liébanas, G., et al. (2016). A new stem nematode, Ditylenchus oncogenus n. sp.(*Nematoda*: *Tylenchida*), parasitizing sowthistle from Adriatic coast dunes in southern Italy. *J. Helminthol.* 90, 152–165. doi: 10.1017/S0022149X14000947

Williams, J. P., Hanavan, R. P., Rock, B. N., Minocha, S. C., and Linder, E. (2016). Influence of hemlock woolly adelgid infestation on the physiological and reflectance characteristics of eastern hemlock. *Can. J. For. Res.* 46, 410–426. doi: 10.1139/cjfr-2015-0328

Xue, Z. Y., and Ullrich, P. A. (2022). Changing trends in drought patterns over the Northeastern United States using multiple large ensemble datasets. *J. Clim.* 35, 3813–3833. doi: 10.1175/JCLI-D-21-0810.1

Ziv, M., and Ariel, T. (1994). "Vitrification in relation to stomatal deformation and malfunction in carnation leaves in vitro," in *Physiology, growth and development of plants in culture*, eds P. J. Lumsden, J. R. Nicholas, and W. J. Davies (Dordrecht: Springer). doi: 10.1007/978-94-011-0790-7_15